

ScoRe-Flow: Complete Distributional Control via Score-Based Reinforcement Learning for Flow Matching

Xiaotian Qiu^{*1,2} Lukai Chen^{*3} Jinhao Li^{3,2} Qi Sun¹ Cheng Zhuo¹ Guohao Dai^{3,4,2}

Abstract

Flow Matching (FM) policies have emerged as an efficient backbone for robotic control, offering fast and expressive action generation that underpins recent large-scale embodied AI systems. However, FM policies trained via imitation learning inherit the limitations of demonstration data; surpassing suboptimal behaviors requires reinforcement learning (RL) fine-tuning. Recent methods convert deterministic flows into stochastic differential equations (SDEs) with learnable noise injection, enabling exploration and tractable likelihoods, but such noise-only control can compromise training efficiency when demonstrations already provide strong priors. We observe that modulating the drift via the score function, i.e., the gradient of log-density, steers exploration toward high-probability regions, improving stability. The score admits a closed-form expression from the velocity field, requiring no auxiliary networks. Based on this, we propose **ScoRe-Flow**, a score-based RL fine-tuning method that combines drift modulation with learned variance prediction to achieve decoupled control over the mean and variance of stochastic transitions. Experiments demonstrate that ScoRe-Flow achieves **2.4× faster convergence** than flow-based SOTA on D4RL locomotion tasks and **up to 5.4% higher success rates** on Robomimic and Franka Kitchen manipulation tasks.

1. Introduction

Generative policies have reshaped robotic control by moving beyond unimodal regression toward modeling rich multimodal action distributions that better reflect the variability

^{*}Equal contribution Work done during an internship at Shanghai Jiao Tong University. ¹Zhejiang University, Hangzhou, China ²Shanghai Innovation Institute ³Shanghai Jiao Tong University, Shanghai, China ⁴Infinigence-AI. Correspondence to: Guohao Dai <daiguohao@sjtu.edu.cn>.

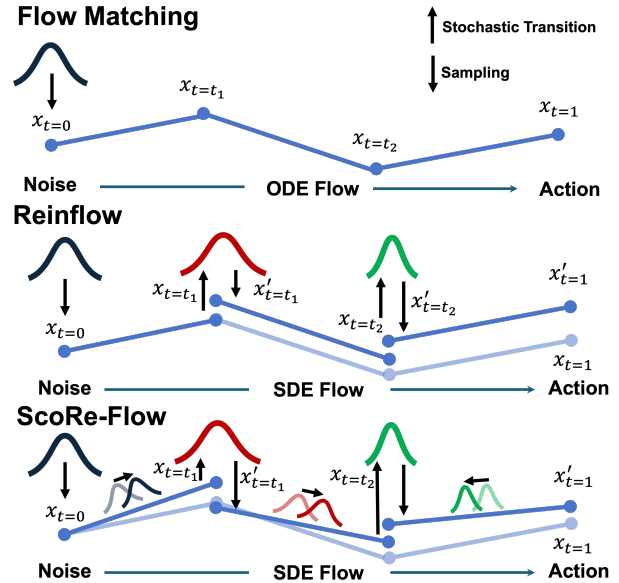


Figure 1. Comparison of flow policy sampling strategies. **Top:** Deterministic FM follows a fixed ODE trajectory with no exploration. **Middle:** Noise-only control (e.g., ReinFlow) injects learnable noise for exploration, but only perturbs the position without modulating dynamics. **Bottom:** ScoRe-Flow combines score-based drift modulation with learned variance prediction, achieving decoupled mean-variance control.

of human demonstrations (Florence et al., 2022; Shafiqul-ah et al., 2022; Pearce et al., 2023; Braun et al.; Zhang & Gienger, 2024). This capability is essential for complex manipulation tasks where multiple valid action sequences can achieve the same goal, and the policy must capture this inherent ambiguity rather than averaging diverse behaviors. Among recent approaches, diffusion-based policies (Chi et al., 2023; Reuss et al., 2023) achieve strong performance through stochastic sampling but often require many iterative denoising steps, limiting their suitability for real-time control and long-horizon decision making.

Flow Matching (FM) provides an ODE-based formulation for action generation, transporting noise to actions along structured trajectories (Lipman et al., 2022; Liu et al., 2023; Albergo & Vanden-Eijnden, 2023). Compared to diffusion models, FM enables significantly faster sampling, typically

requiring 4 to $10\times$ fewer integration steps, while maintaining comparable expressiveness. This formulation has recently been adopted in several large-scale robotic action experts and vision-language-action models (Black et al., 2024; Amin et al., 2025; Chen et al., 2025).

However, most FM policies rely solely on imitation learning (IL) (Albergo et al., 2025), inherently suffering from covariate shift and the performance ceiling of suboptimal demonstrations (Ross et al., 2011). Although RL fine-tuning is essential to transcend these limitations (Rajeswaran et al., 2017), a fundamental challenge arises from the deterministic ODE dynamics of FM: transitions collapse to Dirac measures (Song et al., 2020), rendering action likelihoods ill-defined and precluding direct application of policy gradient methods (Zhang et al., 2025b).

To enable RL fine-tuning of FM policies, recent methods convert deterministic flows into stochastic differential equations (SDEs) with tractable likelihoods (Black et al., 2023; Fan et al., 2024). A representative approach is ReinFlow (Zhang et al., 2025b), which learns an auxiliary network to predict the magnitudes of injected noise at each step of integration. Other concurrent strategies focus on optimizing the input noise distribution to discover high-reward seeds (Yu et al., 2025) or modifying the integrator to mitigate sampling artifacts (Wang & Yu, 2025). Although these methods enable exploration and stabilize fine-tuning, they primarily act through the *noise* component. Concretely, under Euler-Maruyama discretization (Øksendal, 2003), the update $\mathbf{a}_{k+1} = \mathbf{a}_k + \mathbf{v}\Delta t + \sigma\epsilon$ shows that injected noise perturbs the state increment but leaves the drift \mathbf{v} unchanged. This motivates drift modulation as a complementary mechanism for providing directional guidance during sampling.

In this work, we introduce learnable drift modulation for RL fine-tuning of flow policies. Building on the known score-velocity duality for linear flow paths (Albergo & Vanden-Eijnden, 2023; Lipman et al., 2022), we observe that the density gradient (score) can be computed in closed form from the velocity field, enabling score-based drift control without auxiliary networks. Based on this, we propose **ScoRe-Flow** (**Score-based Reinforcement Learning for Flow Matching**), combining score-weighted drift modulation with variance prediction to achieve decoupled control over the mean and variance of stochastic transitions. Empirically, this yields faster convergence on D4RL and improved performance on Robomimic and Franka Kitchen.

In summary, our contributions are threefold as follows:

- We observe that noise-based SDE conversion for FM fine-tuning only perturbs the **position** at each step without modulating the **dynamics** of the flow. The score function, which points toward high-probability regions, provides a principled mechanism to adjust the drift and

steer transitions along geometrically favorable paths.

- Leveraging the known score-velocity duality for linear flow paths (Albergo & Vanden-Eijnden, 2023; Lipman et al., 2022), we propose **ScoRe-Flow**, which uses the **closed-form score** to enable drift modulation requiring **no auxiliary networks and negligible computational overhead**. Combined with variance prediction, this achieves **decoupled control** over the mean and variance of stochastic transitions — a capability absent in existing flow-based RL methods.
- We demonstrate that ScoRe-Flow achieves **$2.4\times$ faster convergence** than the flow-based SOTA (ReinFlow) at matched denoising steps, and **up to 5.4% higher success rates** on sparse-reward Robomimic and Franka Kitchen manipulation tasks. The additional wall-clock advantage over diffusion-based methods ($21.9\times$ over DPPO) is a structural benefit of flow-based sampling shared by all FM methods. Results are validated across state-based and vision-based settings.

2. Related Work

Generative policies for robotic control. Generative models have emerged as powerful backbones for robotic policy learning, offering the ability to capture multimodal action distributions that reflect the inherent variability in human demonstrations (Florence et al., 2022; Shafiullah et al., 2022; Pearce et al., 2023). Diffusion-based policies (Chi et al., 2023; Janner et al., 2022; Reuss et al., 2023) achieve strong performance through iterative denoising, but often require many sampling steps, limiting the applicability in real-time. Flow Matching (FM) (Lipman et al., 2022; Liu et al., 2023; Albergo & Vanden-Eijnden, 2023) provides an ODE-based alternative by learning deterministic velocity fields that transport noise to actions along structured trajectories, enabling significantly faster sampling (often 4 to $10\times$ fewer steps). Recent large-scale robotic systems have adopted FM as the action generation backbone (Black et al., 2024; Amin et al., 2025; Chen et al., 2025).

RL fine-tuning of diffusion and flow policies. Although imitation learning provides robust initialization, reinforcement learning (RL) fine-tuning is essential to exceed demonstration quality (Ball et al., 2023; Ibarz et al., 2021). However, integrating expressive generative policies with RL objectives presents significant challenges, and existing approaches can be broadly categorized by their optimization strategies.

Value-based and Energy-based approaches leverage learned Q-functions or energy landscapes to guide action selection, though these methods typically prioritize offline settings or implicit policy formulations (Hansen-Estruch et al., 2023;

Park et al., 2025; Zhang et al., 2025a). Similarly, other works propose structural modifications to incorporate flow-based networks into actor-critic architectures (Zhong et al., 2025; Bai et al., 2025), tackling distributional matching via architectural redesigns which is different from our objective of enhancing sample efficiency in online fine-tuning through geometric guidance of the flow trajectory

Policy gradient approaches directly optimize the generative policy using likelihood-based objectives. DPPO (Ren et al., 2024) applies PPO to diffusion policies by modeling denoising as a multi-step MDP. For flow policies, ReinFlow (Zhang et al., 2025b) converts the deterministic ODE into an SDE by learning noise injection. Smart-GRPO (Yu et al., 2025) optimizes the input noise distribution to discover high-reward seeds, while Coefficients-Preserving Sampling (Wang & Yu, 2025) modifies the integrator to reduce sampling artifacts. However, these approaches largely focus on optimizing noise parameters or stabilizing numerical integration, rather than leveraging the underlying probability geometry. Additionally, unlike language-domain approaches like FlowRL (Zhu et al., 2025), which prioritize diversity through distribution matching, our framework is tailored for robotic control, focusing on maximizing expected returns to ensure precise and reliable manipulation.

Score functions and guided generation. The score function, i.e., the gradient of log-density, plays a central role in diffusion models (Song & Ermon, 2019; Song et al., 2020) and connects to various guidance techniques for conditional generation (Ho & Salimans, 2022). Recent works have explored using score-based guidance to steer generative trajectories toward desired regions (Sabour et al., 2025; Yuan et al., 2024). The relationship between score and velocity in flow models has been established through stochastic interpolants (Albergo & Vanden-Eijnden, 2023), showing that both encode equivalent information about the probability flow. We leverage this connection to derive a closed-form score expression from the velocity field, enabling drift modulation without auxiliary networks.

3. Preliminaries

Reinforcement learning setup. We consider a Markov Decision Process (MDP) $\mathcal{M} = (\mathcal{S}, \mathcal{A}, \mathcal{P}, \gamma, \mathcal{R}, \mu)$, where \mathcal{S} denotes the state space, $\mathcal{A} = \mathbb{R}^d$ the continuous action space, $\mathcal{P} : \mathcal{S} \times \mathcal{A} \rightarrow \Delta(\mathcal{S})$ the transition dynamics, $\gamma \in [0, 1)$ the discount factor, $\mathcal{R} : \mathcal{S} \times \mathcal{A} \rightarrow \mathbb{R}$ the reward function, and μ the initial state distribution. The objective is to learn a policy $\pi_\theta(\mathbf{a} | \mathbf{s})$ that maximizes the expected discounted return:

$$J(\pi) = \mathbb{E}_{s_0 \sim \mu, a_t \sim \pi(\cdot | s_t), s_{t+1} \sim \mathcal{P}} \left[\sum_{t=0}^{\infty} \gamma^t \mathcal{R}(s_t, a_t) \right]. \quad (1)$$

In offline-to-online RL, we first pre-train a policy via imitation learning on an offline dataset $\mathcal{D} = \{(s_i, a_i)\}_{i=1}^{|\mathcal{D}|}$, then fine-tune through online interaction to exceed demonstration performance.

Policy gradient and PPO. Policy gradient methods optimize $J(\pi)$ by estimating gradients with respect to policy parameters. The REINFORCE estimator (Williams, 1992) computes $\nabla_\theta J(\pi) = \mathbb{E}_\pi[\nabla_\theta \log \pi_\theta(\mathbf{a} | \mathbf{s}) \cdot A^\pi(\mathbf{s}, \mathbf{a})]$, where A^π is the advantage function. This requires the policy to define a valid probability density $\pi_\theta(\mathbf{a} | \mathbf{s})$ over actions with tractable log-likelihood. Proximal Policy Optimization (PPO) (Schulman et al., 2017) stabilizes training by constraining policy updates via a clipped surrogate:

$$\mathcal{L}^{\text{PPO}}(\theta) = \mathbb{E}[\min(r_t(\theta)A_t, \text{clip}(r_t(\theta), 1 - \epsilon, 1 + \epsilon)A_t)], \quad (2)$$

where $r_t(\theta) = \pi_\theta(\mathbf{a}_t | \mathbf{s}_t) / \pi_{\theta_{\text{old}}}(\mathbf{a}_t | \mathbf{s}_t)$ is the probability ratio. PPO is widely used for fine-tuning generative policies due to its stability and sample efficiency.

Flow Matching. Flow Matching (FM) (Lipman et al., 2022) learns a time-dependent velocity field $\mathbf{v}_\theta : \mathbb{R}^d \times [0, 1] \rightarrow \mathbb{R}^d$ that transforms noise samples $\mathbf{a}_0 \sim \mathcal{N}(\mathbf{0}, \mathbf{I})$ into data samples $\mathbf{a}_1 \sim p_{\text{data}}$ through a continuous-time process. The linear interpolation between noise and data is given by $\mathbf{a}_t = (1 - t)\mathbf{a}_0 + t\mathbf{a}_1$ for $t \in [0, 1]$. The model learns to approximate this process by solving the ordinary differential equation (ODE) $d\mathbf{a}_t = \mathbf{v}_\theta(\mathbf{a}_t, t)dt$, and is trained using the flow matching objective:

$$\mathcal{L}_{\text{FM}}(\theta) = \mathbb{E}_{t, \mathbf{a}_0, \mathbf{a}_1} \left[\|\mathbf{v}_\theta(\mathbf{a}_t, t) - (\mathbf{a}_1 - \mathbf{a}_0)\|_2^2 \right], \quad (3)$$

where $t \sim \mathcal{U}[0, 1]$, $\mathbf{a}_0 \sim \mathcal{N}(\mathbf{0}, \mathbf{I})$, and $\mathbf{a}_1 \sim p_{\text{data}}$. For policy learning, the velocity field is conditioned on observations: $\mathbf{v}_\theta(\mathbf{a}_t, t, \mathbf{s})$.

4. Method

We present ScoRe-Flow, a method for RL fine-tuning of Flow Matching policies that achieves decoupled control over the mean and variance of stochastic transitions. We first derive a closed-form score expression from the velocity field (Section 4.1), then introduce ScoRe-Flow which combines score-based drift modulation with learned variance prediction (Section 4.2).

4.1. Closed-Form Score from Velocity

As discussed in Section 3, converting the deterministic FM dynamics to an SDE enables tractable likelihood computation for policy gradient methods. The general SDE formulation $d\mathbf{a}_t = \boldsymbol{\mu}(\mathbf{a}_t, t)dt + \sigma(\mathbf{a}_t, t)d\mathbf{W}_t$ provides flexibility in designing both the drift $\boldsymbol{\mu}$ and diffusion σ . Existing methods such as ReinFlow (Zhang et al., 2025b)

set $\boldsymbol{\mu} = \mathbf{v}_\theta$ (the pre-trained velocity) and learn only σ . However, from a kinematic perspective, the discrete update $\mathbf{a}_{k+1} = \mathbf{a}_k + \mathbf{v}\Delta t + \sigma\epsilon$ reveals that the noise term $\sigma\epsilon$ only perturbs the current position without modulating the dynamics of the flow itself. This motivates us to explore whether modulating the drift can provide additional benefits.

Score function. To enable drift modulation without training additional networks, we leverage the *score function*, i.e., the gradient of the log-density of intermediate marginals (Song et al., 2020). Let $\rho_t(\mathbf{a})$ denote the marginal density of the flow at time t . The score function is defined as

$$\mathbf{s}_t(\mathbf{a}) \triangleq \nabla_{\mathbf{a}} \log \rho_t(\mathbf{a}), \quad (4)$$

which points toward regions of higher probability density in the intermediate marginal, providing a natural direction for steering transitions toward the data manifold.

Derivation. For the linear FM path $\mathbf{a}_t = (1-t)\mathbf{a}_0 + t\mathbf{a}_1$ with $\mathbf{a}_0 \sim \mathcal{N}(\mathbf{0}, \mathbf{I})$ and $\mathbf{a}_1 \sim p_{\text{data}}$, the intermediate marginal ρ_t is a convolution of the data distribution with Gaussian noise of variance $(1-t)^2\mathbf{I}$. By analyzing the relationship between the optimal velocity and the conditional expectation, we derive a closed-form expression for the score in terms of the velocity field (see Appendix A for the complete derivation):

$$\mathbf{s}_t(\mathbf{a}) = \frac{t \mathbf{v}_\theta(t, \mathbf{a}, \mathbf{s}) - \mathbf{a}}{1-t}. \quad (5)$$

This *score-velocity duality* is established in the stochastic interpolant literature (Albergo & Vanden-Eijnden, 2023; Albergo et al., 2025), where the score and velocity are shown to encode equivalent information about the underlying probability flow (see also Lipman et al. (2022), Eq. 4.78). Our contribution is not the identity itself, but the observation that it enables practical drift modulation for RL fine-tuning of flow policies: the score can be computed directly from the pre-trained velocity field via a simple algebraic transformation, requiring zero additional parameters and negligible computational overhead, enabling decoupled control over the mean and variance of stochastic transitions.

Consistent with the boundary divergence issues noted in Elucidating Diffusion Models (Karras et al., 2022), a critical practical consideration is that the score magnitude diverges as $|\mathbf{s}_t(\mathbf{a})| = O((1-t)^{-1})$ near $t = 1$. Therefore, the coefficient multiplying the score in the drift must decay as $O(1-t)$ to keep the score-corrected drift bounded. In ScoRe-Flow, we enforce this property via a hard time-decay constraint on the score scheduler:

$$\alpha_\psi^{\text{scaled}}(t) \triangleq (1-t) \alpha_\psi(t), \quad (6)$$

so that $\alpha_\psi^{\text{scaled}} \rightarrow 0$ as $t \rightarrow 1$ and the score-modulated drift remains numerically stable.

Algorithm 1 ScoRe-Flow: Action Sampling with Decoupled Mean-Variance Control

- 1: **Input:** Observation \mathbf{s} , pre-trained velocity \mathbf{v}_θ , learnable networks α_ψ, σ_ϕ , steps K
 - 2: Sample initial noise: $\mathbf{a} \sim \mathcal{N}(\mathbf{0}, \mathbf{I})$
 - 3: Initialize log-probability: $\log p \leftarrow 0$
 - 4: **for** $k = 0, 1, \dots, K - 1$ **do**
 - 5: Compute time step: $t \leftarrow k/K, \Delta t \leftarrow 1/K$
 - 6: Evaluate velocity field: $\mathbf{v} \leftarrow \mathbf{v}_\theta(\mathbf{a}, t, \mathbf{s})$
 - 7: Compute closed-form score: $\mathbf{s}_{\text{score}} \leftarrow (t \cdot \mathbf{v} - \mathbf{a}) / (1 - t)$
 - 8: Predict learnable weights: $\alpha \leftarrow \alpha_\psi(t), \sigma \leftarrow \sigma_\phi(\mathbf{a}, t, \mathbf{s})$
 - 9: Apply time-decay: $\alpha_{\text{scaled}} \leftarrow (1 - t) \cdot \alpha$
 - 10: Compute transition mean: $\boldsymbol{\mu} \leftarrow \mathbf{a} + (\mathbf{v} + \alpha_{\text{scaled}} \cdot \mathbf{s}_{\text{score}}) \cdot \Delta t$
 - 11: Sample noise and update: $\epsilon \sim \mathcal{N}(\mathbf{0}, \mathbf{I}), \mathbf{a} \leftarrow \boldsymbol{\mu} + \sigma \cdot \sqrt{\Delta t} \cdot \epsilon$
 - 12: Accumulate log-probability: $\log p \leftarrow \log p + \log \mathcal{N}(\mathbf{a}; \boldsymbol{\mu}, \sigma^2 \Delta t \cdot \mathbf{I})$
 - 13: **end for**
 - 14: **Return:** Final action \mathbf{a} , trajectory log-probability $\log p$
-

4.2. ScoRe-Flow: Decoupled Mean and Variance Control

With the closed-form score in hand, we now present ScoRe-Flow, which combines score-weighted drift modulation with learned variance prediction to achieve decoupled control over the first two moments of each transition kernel.

Noise-only methods learn σ to control the magnitude of the exploration (Zhang et al., 2025b), but the noise term only perturbs the position at each step without modulating the underlying dynamics. Intuitively, this resembles adding random perturbations to a particle’s location rather than adjusting its velocity. While effective for enabling exploration and likelihood computation, this approach does not leverage the geometric structure of the flow. In contrast, modulating the drift via the score, which points toward high-density regions consistent with the principles of Langevin Dynamics (Welling & Teh, 2011), can provide directional guidance that complements variance control, improving stability when trajectories enter low-density regions and accelerating convergence when the pre-trained trajectory is already informative. However, standard score-based control rigidly couples the drift and diffusion terms (e.g., a drift of $\lambda(t)\mathbf{s}_t$ requires variance $\sqrt{2\lambda(t)}$ to maintain equilibrium), preventing independent adjustment of exploration magnitude and intensity required for effective RL fine-tuning.

ScoRe-Flow decouples drift and variance control by introducing two learnable components: a score scheduler $\alpha_\psi^{\text{scaled}}$ (with hard time decay from Equation (6)) that modulates

the score-based drift correction, and a variance predictor σ_ϕ that independently determines the exploration magnitude. The resulting SDE takes the form:

$$d\mathbf{a}_t = \left[\mathbf{v}_\theta(t, \mathbf{a}_t, \mathbf{s}) + \alpha_\psi^{\text{scaled}}(t) \cdot \mathbf{s}_t(\mathbf{a}_t) \right] dt + \sigma_\phi(t, \mathbf{a}_t, \mathbf{s}) d\mathbf{W}_t, \quad (7)$$

where \mathbf{v}_θ is the FM velocity field (initialized from pre-training and jointly optimized during fine-tuning), \mathbf{s}_t is the closed-form score from Equation (5), $\alpha_\psi^{\text{scaled}}$ is the score scheduler with endpoint stabilization from Equation (6), and $\sigma_\phi : \mathbb{R}^d \times [0, 1] \times \mathcal{S} \rightarrow \mathbb{R}^+$ is the learnable variance prediction network.

The key insight of ScoRe-Flow is the decomposition of distributional control into two complementary mechanisms. The score-modulated drift term $\alpha_\psi^{\text{scaled}} \cdot \mathbf{s}_t$ leverages the score to provide geometrically meaningful guidance toward higher-probability regions under the flow marginal. When the exploration trajectory wanders into low-density areas, the score acts as a corrective force steering it back toward the data manifold. The score scheduler $\alpha_\psi^{\text{scaled}}(t)$ adaptively determines the strength of this correction based on the time step, while satisfying the endpoint stability constraint via the $(1-t)$ decay. Meanwhile, the variance term σ_ϕ governs the magnitude of stochastic exploration independently of its direction. This decoupling enables the policy to, for example, maintain strong drift correction while reducing exploration noise as training progresses, or vice versa. Such flexibility is unattainable by noise-only or score-only methods.

Discrete-time formulation. For practical implementation, we discretize Equation (7) using the Euler-Maruyama scheme with K integration steps. Let $t_k = k/K$ and $\Delta t = 1/K$ for $k = 0, 1, \dots, K-1$. The discrete update rule is:

$$\mathbf{a}^{k+1} = \mathbf{a}^k + \left[\mathbf{v}_\theta^k + (\alpha_\psi^{\text{scaled}})^k \cdot \mathbf{s}^k \right] \Delta t + \sigma_\phi^k \sqrt{\Delta t} \epsilon_k, \quad (8)$$

where $\epsilon_k \sim \mathcal{N}(\mathbf{0}, \mathbf{I})$ is standard Gaussian noise, and we use the shorthand $\mathbf{v}_\theta^k = \mathbf{v}_\theta(t_k, \mathbf{a}^k, \mathbf{s})$, $(\alpha_\psi^{\text{scaled}})^k = (1-t_k)\alpha_\psi(t_k)$, $\mathbf{s}^k = \mathbf{s}_{t_k}(\mathbf{a}^k)$, and $\sigma_\phi^k = \sigma_\phi(t_k, \mathbf{a}^k, \mathbf{s})$.

Likelihood computation. Each transition follows a Gaussian distribution with mean $\boldsymbol{\mu}^k = \mathbf{a}^k + [\mathbf{v}_\theta^k + (\alpha_\psi^{\text{scaled}})^k \mathbf{s}^k] \Delta t$ and variance $(\sigma_\phi^k)^2 \Delta t$:

$$p(\mathbf{a}^{k+1} | \mathbf{a}^k, \mathbf{s}) = \mathcal{N}\left(\mathbf{a}^{k+1}; \boldsymbol{\mu}^k, (\sigma_\phi^k)^2 \Delta t \mathbf{I}\right). \quad (9)$$

The trajectory log-likelihood factorizes as:

$$\log \pi(\mathbf{a}_1 | \mathbf{s}) = \sum_{k=0}^{K-1} \log p(\mathbf{a}^{k+1} | \mathbf{a}^k, \mathbf{s}), \quad (10)$$

which can be computed in closed form, enabling direct application of PPO for policy optimization.

Implementation. The drift modulation weight $\alpha_\psi(t)$ is implemented as a lightweight MLP that takes only the scalar time step t as input. The variance predictor σ_ϕ is an independent MLP that takes the concatenation of the current action \mathbf{a}_t , time step t , and observation \mathbf{s} (or its encoded representation for image observations). During RL fine-tuning, we adopt a full parameter fine-tuning strategy. Instead of freezing the base model, we jointly optimize the pre-trained velocity field \mathbf{v}_θ alongside the parameters ψ and ϕ of the drift modulation and variance networks using PPO, maximizing the trajectory log-likelihood defined in Eq. 10. The hard time-decay constraint in Equation (6) ensures that the score correction is strongest in the early stages of the flow and diminishes toward the endpoint, preventing instability from the $(1-t)^{-1}$ scaling of the score. Complete architecture specifications and hyperparameter settings are provided in Appendix B and C.

5. Experiments

We evaluate ScoRe-Flow on continuous control benchmarks spanning locomotion and manipulation to answer: (i) Does combining score-based mean control with variance prediction outperform either component alone? (ii) How does ScoRe-Flow compare with state-of-the-art methods?

5.1. Environments

We evaluate on three benchmark suites.

D4RL Locomotion (Fu et al., 2020) comprises OpenAI Gym MuJoCo tasks including Hopper-v2, Walker2d-v2, Ant-v0, and Humanoid-v3, where we use the medium-expert datasets for pre-training. These tasks provide dense rewards and test the ability to learn efficient locomotion gaits beyond suboptimal demonstrations.

Robomimic (Mandlekar et al., 2021) consists of visual manipulation tasks including PickPlaceCan (single-arm pick-and-place), Square (precise peg insertion) and Transport (bi-manual coordination), with 96×96 RGB image observations and proficient-human (ph) demonstrations for pre-training.

Franka Kitchen (Gupta et al., 2019) is a benchmark environment for sequential multi-task manipulation, which includes tasks such as opening a microwave, repositioning a kettle, activating a light switch, and sliding a cabinet door using a Franka Panda robotic arm. We perform evaluations on the complete, mixed, and partial dataset variants under a sparse reward formulation in which a unit reward is granted upon successful completion of each subtask.

5.2. Baselines

We compare ScoRe-Flow against the following methods.

ReinFlow (Zhang et al., 2025b) introduces learnable vari-

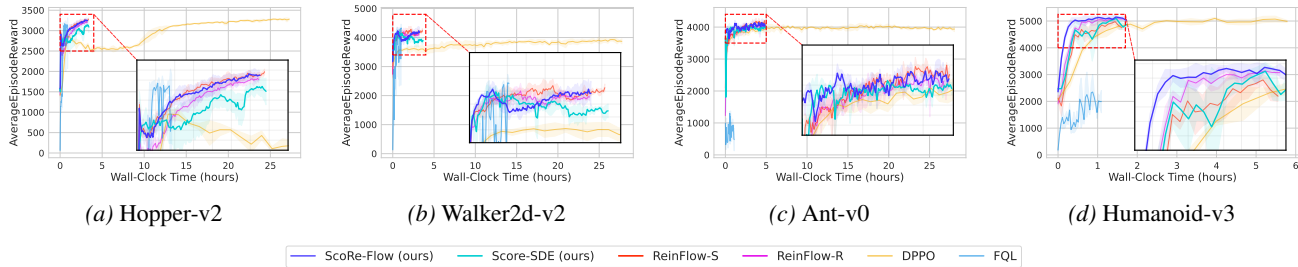


Figure 2. Learning curves on D4RL locomotion tasks. Dashed lines indicate the behavior cloning level.

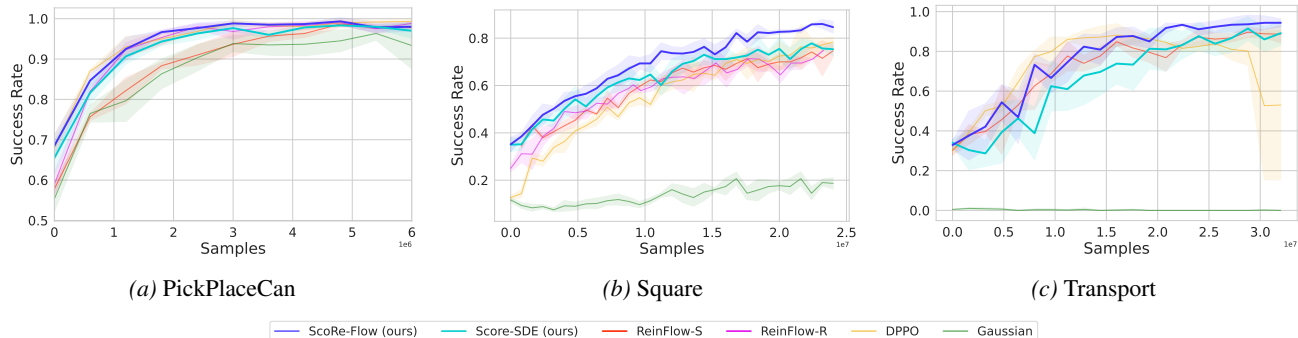


Figure 3. Learning curves on Robomimic visual manipulation tasks.

ance prediction for flow policy RL. We evaluate two variants: **ReinFlow-R** uses Rectified Flow as the base policy with 4 denoising steps, representing the variance-only control paradigm; **ReinFlow-S** uses Shortcut Model as the base policy with 1 to 4 denoising steps and learned step-skipping for improved efficiency.

DPPO (Ren et al., 2024) applies Diffusion Policy (Chi et al., 2023) with PPO fine-tuning, using DDIM sampling with 50 to 100 denoising steps at higher computational cost but achieving strong performance on diffusion policies.

FQL (Park et al., 2025) implements Flow Q-Learning with offline training and distillation, lacking online exploration during the fine-tuning phase.

Ablation Method. **Score-SDE** is a simplified variant that uses only score-based mean control without learned variance prediction. In this ablation, the same schedule $\lambda(t)$ determines both the drift correction strength and the diffusion magnitude. Specifically, it follows the SDE:

$$d\mathbf{a}_t = \left[\mathbf{v}_\theta + \lambda(t) \cdot \mathbf{s}_t(\mathbf{a}_t) \right] dt + \sqrt{2\lambda(t)} d\mathbf{W}_t, \quad (11)$$

where the diffusion coefficient is coupled to the drift schedule as $\sigma(t) = \sqrt{2\lambda(t)}$. This formulation corresponds to a time-reversal of the forward noising process. By comparing Score-SDE to ScoRe-Flow, we isolate the contribution of decoupled variance prediction.

Pre-trained Policies. To ensure a rigorous comparison, we strictly align our pre-training setup with ReinFlow (Zhang et al., 2025b). Specifically, we initialize our base policies using identical pre-trained weights and model architectures, adopting either Rectified Flow or Shortcut Models based on the optimal configuration reported in their work. All policies are trained using the standard Flow Matching objective on respective demonstration data.

Implementation Details. We adopt a task-dependent architecture for the pre-trained base policy, employing **Rectified Flow** for D4RL and simpler Robomimic tasks, and **Shortcut Models** for long-horizon tasks (Franka Kitchen, Transport) to maximize efficiency. For fine-tuning, we generally set the denoising steps $K = 4$, with exceptions for specific tasks to balance performance and cost. The exploration process is governed by a learnable noise scheduler or a fixed hold strategy depending on the domain. Comprehensive hyperparameters, including network architectures and detailed optimization settings, are provided in Tables 2 to 5.

5.3. Results

Table 1 summarizes the quantitative results in all benchmarks. Figures 2, 3, and 4 show the corresponding learning curves. Detailed configurations and rationale for the selection of the backbone model, based on the settings and training performance reported in ReinFlow (Zhang et al., 2025b), are provided in Table 7 in Appendix D.

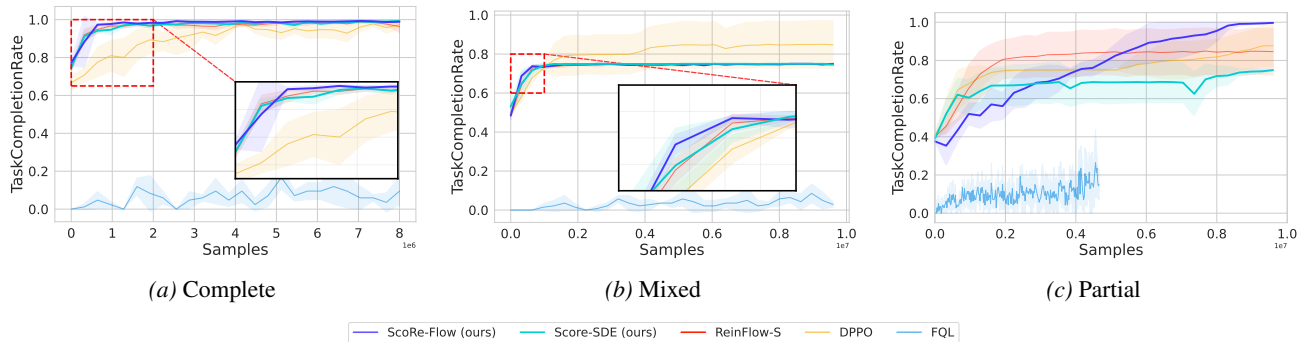


Figure 4. Learning curves on Franka Kitchen multi-task benchmark.

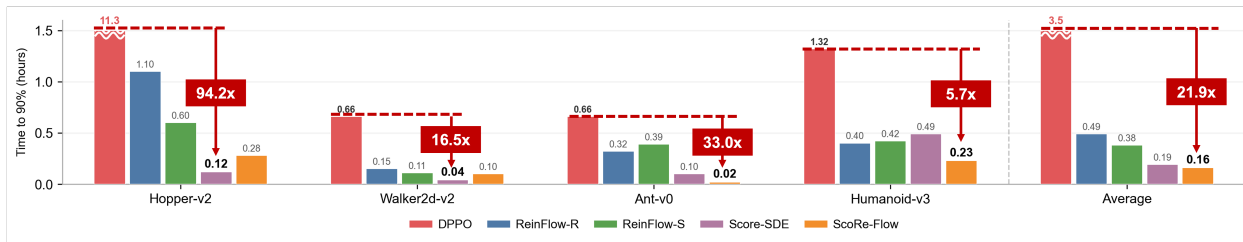


Figure 5. Wall-clock time comparison on D4RL locomotion tasks. The large speedup over DPPO (up to $94.2\times$ on Hopper-v2, $21.9\times$ average) is primarily a structural advantage of flow-based methods requiring fewer denoising steps. The algorithmic contribution is the $2.4\times$ faster convergence over the flow-based baseline ReinFlow at matched $K = 4$ steps.

Table 1. Performance comparison across all benchmarks. We report final performance (mean \pm std over 3 seeds). The BC (pretrain) column indicates the baseline performance of the behavior cloning policy before fine-tuning. **Bold**: best, underline: second best.

Task	BC (pretrain)	DPPO	ReinFlow-R	ReinFlow-S	Score-SDE	ScoRe-Flow (Ours)
<i>D4RL Locomotion (Episode Reward \uparrow)</i>						
Hopper-v2	1578 \pm 28	3275\pm20	3204 \pm 36	<u>3253\pm24</u>	3118 \pm 87	3233 \pm 39
Walker2d-v2	3185 \pm 38	3896 \pm 62	4092 \pm 11	4202\pm26	3900 \pm 57	<u>4172\pm154</u>
Ant-v0	3750 \pm 118	3951 \pm 24	4021 \pm 25	4119\pm44	3980 \pm 29	<u>4088\pm95</u>
Humanoid-v3	2415 \pm 65	5001 \pm 20	<u>5041\pm6</u>	4801 \pm 134	4896 \pm 91	5100\pm47
Avg.	2732	4031	4090	<u>4094</u>	3974	4148
<i>Robomimic (Success Rate % \uparrow)</i>						
PickPlaceCan	68.0 \pm 1.8	96.5 \pm 0.2	95.6 \pm 0.1	91.7 \pm 0.5	96.8 \pm 0.2	98.3\pm0.5
Square	33.3 \pm 2.8	<u>78.3\pm2.0</u>	76.2 \pm 2.0	77.3 \pm 2.1	75.3 \pm 2.6	84.7\pm2.5
Transport	27.0 \pm 3.6	53.0 \pm 37.7	N/A	88.7 \pm 4.4	<u>89.2\pm6.1</u>	94.4\pm2.0
Avg.	42.8	75.9	N/A	85.9	<u>87.1</u>	92.5
<i>Franka Kitchen (Tasks Completed, max 4 \uparrow)</i>						
Complete	3.03 \pm 0.1	3.8 \pm 0.1	N/A	3.9 \pm 0.0	4.0\pm0.0	4.0\pm0.0
Mixed	2.04 \pm 0.1	3.4\pm0.5	N/A	3.0 \pm 0.0	3.0 \pm 0.0	3.0 \pm 0.0
Partial	1.53 \pm 0.1	3.3 \pm 0.4	N/A	<u>3.4\pm0.5</u>	2.8 \pm 0.2	3.8\pm0.2
Avg.	2.20	<u>3.50</u>	N/A	3.43	3.27	3.60

D4RL Locomotion. ScoRe-Flow achieves the highest average performance across all D4RL tasks, outperforming both the ReinFlow variants and DPPO. In particular, ScoRe-Flow excels in the challenging Humanoid-v3 task with 5100 ± 47 reward, surpassing all baselines including the strong ReinFlow-R (5041) and DPPO (5001). In terms

of efficiency, ScoRe-Flow achieves an average time-to-convergence of just 0.16 hours to reach 90% of the final performance, compared to DPPO’s 3.48-hour average. We note that this wall-clock speedup is primarily a *structural* advantage shared by all flow-based methods over diffusion-based methods, as flow policies require only 2–4 denoising

steps versus the 50–100 steps typical of DPPO. More relevant to our algorithmic contribution, ScoRe-Flow achieves $2.4\times$ faster convergence than the flow-based SOTA (ReinFlow) at the same $K = 4$ denoising steps. We attribute this to the score-based drift modulation, which provides per-step geometric guidance toward high-density regions, accelerating early-stage learning before \mathbf{v}_θ is well-calibrated.

Robomimic. ScoRe-Flow consistently outperforms all baselines in PickPlaceCan, Square, and Transport tasks, achieving the highest success rates while maintaining competitive training efficiency. Despite challenges posed by visual observations, our score-based mean control effectively guides exploration in high-dimensional image spaces.

Franka Kitchen. Despite the challenging multi-task setting with sparse rewards, ScoRe-Flow achieves substantial improvements over baselines, demonstrating the effectiveness of our unified mean-variance control. The Score-SDE ablation achieves faster convergence but lower final performance, confirming that combining score-based mean control with learned variance prediction yields the optimal balance.

Evaluation Protocol. Table 1 summarizes quantitative performance, reporting episode rewards for D4RL locomotion and success rates for Robomimic manipulation. For Franka Kitchen, the table details average subtasks completed out of 4 to highlight granularity, while Figure 4 plots the success rate normalized to $[0, 1]$ for visualizing convergence. All methods use identical pre-trained policy initialization and computational budget for fair comparison.

6. Analysis

Training Stability Comparison. A key advantage of ScoRe-Flow is improved training stability. Figure 6 compares learning dynamics on Kitchen-Complete using Rectified Flow. While ReinFlow exhibits unstable learning with high variance, ScoRe-Flow maintains stable improvement throughout training. This stability stems from score-based mean control, which provides geometrically grounded guidance preventing the policy from drifting into low-probability regions.

Sensitivity of Score-Only Methods to Noise Variance. Using Score-SDE alone without learned variance prediction makes the method highly sensitive to manually specified noise variance σ^2 . Figure 7 shows Score-SDE performance under different fixed σ on Ant-v0. The optimal σ varies significantly between tasks: too small leads to insufficient exploration, while too large causes instability. ScoRe-Flow learns variance adaptively through σ_ϕ , eliminating task-specific tuning.

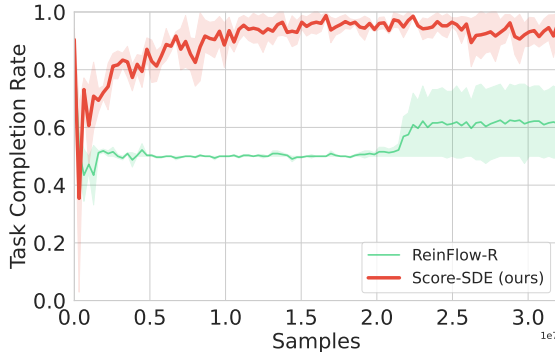


Figure 6. Training stability comparison on Kitchen-Complete-v0. Under the same Rectified Flow base policy, ScoRe-Flow achieves stable learning while ReinFlow exhibits high variance and unstable convergence behavior.

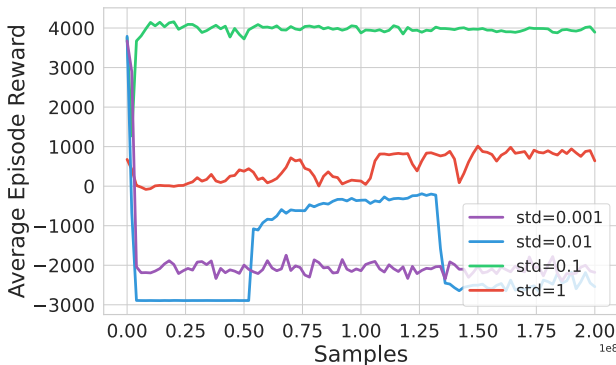


Figure 7. Sensitivity of Score-SDE to initial noise variance. Performance varies dramatically with different fixed σ values, demonstrating that score-only methods require careful task-specific tuning.

Additional Ablation Studies. We provide comprehensive ablation studies in Appendix D, analyzing the impact of denoising steps (K) and the decoupled variance prediction mechanism. Results show that while Score-SDE’s rigid linear decay offers fast initial convergence, it lacks adaptability and yields lower asymptotic performance than ScoRe-Flow’s learned variance.

7. Conclusion

We presented ScoRe-Flow, a method for RL fine-tuning of Flow Matching policies achieving decoupled mean-variance control. Building on the known score-velocity duality for linear flow paths (Albergo & Vanden-Eijnden, 2023; Lipman et al., 2022), we enable score-based drift modulation with negligible overhead. Combined with learned variance prediction, ScoRe-Flow independently adjusts exploration direction and magnitude. Experiments demonstrate faster convergence and improved performance over variance-only and score-only baselines.

Limitations. The closed-form score expression (Eq. 5) relies on the Gaussian conditional structure of linear interpolation paths with a Gaussian source distribution. For non-linear flow paths (e.g., Riemannian Flow Matching) or non-Gaussian source distributions, the conditional density is no longer Gaussian, and the score would require approximate or learned estimation — potentially losing the zero-auxiliary-network advantage. Linear paths cover the dominant use case in current robotic control applications (Lipman et al., 2022; Zhang et al., 2025b), but extending to general stochastic interpolants (Albergo & Vanden-Eijnden, 2023) is an important direction for future work.

Impact Statement

This paper presents work whose goal is to advance the field of Machine Learning. There are many potential societal consequences of our work, none which we feel must be specifically highlighted here.

References

- Albergo, M., Boffi, N. M., and Vanden-Eijnden, E. Stochastic interpolants: A unifying framework for flows and diffusions. *Journal of Machine Learning Research*, 26 (209):1–80, 2025.
- Albergo, M. S. and Vanden-Eijnden, E. Stochastic interpolants: A unifying framework for flows and diffusions. *arXiv preprint arXiv:2303.08797*, 2023.
- Amin, A., Aniceto, R., Balakrishna, A., Black, K., Conley, K., Connors, G., Darpinian, J., Dhabalia, K., DiCarlo, J., Driess, D., et al. $\pi_{0,6}$: a vla that learns from experience. *arXiv preprint arXiv:2511.14759*, 2025.
- Bai, W., Zhang, C., Fu, Y., Zhao, P., and Qian, H. Pacer: A fully push-forward-based distributional reinforcement learning algorithm. *Neurocomputing*, pp. 131301, 2025.
- Ball, P. J., Smith, L., Kostrikov, I., and Levine, S. Efficient online reinforcement learning with offline data. In *International Conference on Machine Learning*, pp. 1577–1594. PMLR, 2023.
- Black, K., Janner, M., Du, Y., Kostrikov, I., and Levine, S. Training diffusion models with reinforcement learning. *arXiv preprint arXiv:2305.13301*, 2023.
- Black, K., Brown, N., Driess, D., Esmail, A., Equi, M., Finn, C., Fusai, N., Groom, L., Hausman, K., Ichter, B., et al. π_0 : A vision-language-action flow model for general robot control. *arXiv preprint arXiv:2410.24164*, 2024.
- Braun, M., Jaquier, N., Rozo, L., and Asfour, T. Riemannian flow matching policy for robot motion learning. in 2024 IEEE. In *RSJ International Conference on Intelligent Robots and Systems (IROS)*, pp. 5144–5151.
- Chen, K., Liu, Z., Zhang, T., Guo, Z., Xu, S., Lin, H., Zang, H., Zhang, Q., Yu, Z., Fan, G., et al. π_{RL} : Online rl fine-tuning for flow-based vision-language-action models. *arXiv preprint arXiv:2510.25889*, 2025.
- Chi, C., Feng, S., Du, Y., Xu, Z., Cousineau, E., Burchfiel, B., and Song, S. Diffusion policy: Visuomotor policy learning via action diffusion. In *Robotics: Science and Systems (RSS)*, 2023.
- Fan, Y. et al. Denoising diffusion policy optimization. *ICLR*, 2024.
- Florence, P., Lynch, C., Zeng, A., Ramirez, O. A., Wahid, A., Downs, L., Wong, A., Lee, J., Mordatch, I., and Tompson, J. Implicit behavioral cloning. In *Conference on robot learning*, pp. 158–168. PMLR, 2022.
- Fu, J., Kumar, A., Nachum, O., Tucker, G., and Levine, S. D4rl: Datasets for deep data-driven reinforcement learning. *arXiv preprint arXiv:2004.07219*, 2020.
- Gupta, A., Kumar, V., Lynch, C., Levine, S., and Hausman, K. Relay policy learning: Solving long-horizon tasks via imitation and reinforcement learning. *arXiv preprint arXiv:1910.11956*, 2019.
- Hansen-Estruch, P., Kostrikov, I., Janner, M., Kuba, J. G., and Levine, S. Idql: Implicit q-learning as an actor-critic method with diffusion policies. *arXiv preprint arXiv:2304.10573*, 2023.
- Ho, J. and Salimans, T. Classifier-free diffusion guidance. *arXiv preprint arXiv:2207.12598*, 2022.
- Ibarz, J., Tan, J., Finn, C., Kalakrishnan, M., Pastor, P., and Levine, S. How to train your robot with deep reinforcement learning: lessons we have learned. *The International Journal of Robotics Research*, 40(4-5):698–721, 2021.
- Janner, M., Du, Y., Tenenbaum, J. B., and Levine, S. Planning with diffusion for flexible behavior synthesis. *arXiv preprint arXiv:2205.09991*, 2022.
- Karras, T., Aittala, M., Aila, T., and Laine, S. Elucidating the design space of diffusion-based generative models. *Advances in neural information processing systems*, 35: 26565–26577, 2022.
- Kingma, D. P. Adam: A method for stochastic optimization. *arXiv preprint arXiv:1412.6980*, 2014.
- Lai, L., Huang, A. Z., and Gershman, S. J. Action chunking as conditional policy compression. 2022.

- Lipman, Y., Chen, R. T., Ben-Hamu, H., Nickel, M., and Le, M. Flow matching for generative modeling. *arXiv preprint arXiv:2210.02747*, 2022.
- Liu, X., Gong, C., and Liu, Q. Flow straight and fast: Learning to generate with rectified flow. *ICLR*, 2023.
- Loshchilov, I. and Hutter, F. Sgdr: Stochastic gradient descent with warm restarts. *arXiv preprint arXiv:1608.03983*, 2016.
- Mandlekar, A., Xu, D., Wong, J., Nasiriany, S., Wang, C., Kulkarni, R., Fei-Fei, L., Savarese, S., Zhu, Y., and Martín-Martín, R. What matters in learning from offline human demonstrations for robot manipulation. *arXiv preprint arXiv:2108.03298*, 2021.
- Øksendal, B. *Stochastic Differential Equations: An Introduction with Applications*. Springer, 6th edition, 2003.
- Park, S., Li, Q., and Levine, S. Flow q-learning. *arXiv preprint arXiv:2502.02538*, 2025.
- Pearce, T., Rashid, T., Kanervisto, A., Bignell, D., Sun, M., Georgescu, R., Macua, S. V., Tan, S. Z., Momennejad, I., Hofmann, K., et al. Imitating human behaviour with diffusion models. *ICLR*, 2023.
- Rajeswaran, A., Kumar, V., Gupta, A., Vezhani, G., Schulman, J., Todorov, E., and Levine, S. Learning complex dexterous manipulation with deep reinforcement learning and demonstrations. *arXiv preprint arXiv:1709.10087*, 2017.
- Ren, A. Z., Lidard, J., Ankile, L. L., Simeonov, A., Agrawal, P., Majumdar, A., Burchfiel, B., Dai, H., and Simchowitz, M. Diffusion policy optimization. *arXiv preprint arXiv:2409.00588*, 2024.
- Reuss, M. et al. Goal-conditioned imitation learning using score-based diffusion policies. In *RSS*, 2023.
- Ross, S., Gordon, G., and Bagnell, D. A reduction of imitation learning and structured prediction to no-regret online learning. In *Proceedings of the fourteenth international conference on artificial intelligence and statistics*, pp. 627–635. JMLR Workshop and Conference Proceedings, 2011.
- Sabour, A., Albergo, M. S., Domingo-Enrich, C., Boffi, N. M., Fidler, S., Kreis, K., and Vanden-Eijnden, E. Test-time scaling of diffusions with flow maps. *arXiv preprint arXiv:2511.22688*, 2025.
- Schulman, J., Moritz, P., Levine, S., Jordan, M., and Abbeel, P. High-dimensional continuous control using generalized advantage estimation. *arXiv preprint arXiv:1506.02438*, 2015.
- Schulman, J., Wolski, F., Dhariwal, P., Radford, A., and Klimov, O. Proximal policy optimization algorithms. *arXiv preprint arXiv:1707.06347*, 2017.
- Shafullah, N. M., Cui, Z., Altanzaya, A. A., and Pinto, L. Behavior transformers: Cloning k modes with one stone. *Advances in neural information processing systems*, 35: 22955–22968, 2022.
- Song, Y. and Ermon, S. Generative modeling by estimating gradients of the data distribution. *Advances in neural information processing systems*, 32, 2019.
- Song, Y., Sohl-Dickstein, J., Kingma, D. P., Kumar, A., Ermon, S., and Poole, B. Score-based generative modeling through stochastic differential equations. *arXiv preprint arXiv:2011.13456*, 2020.
- Wang, F. and Yu, Z. Coefficients-preserving sampling for reinforcement learning with flow matching. *arXiv preprint arXiv:2509.05952*, 2025.
- Welch, B. L. The generalization of students ratio. *Annals of Mathematical Statistics*, 18(1):1–35, 1947.
- Welling, M. and Teh, Y. W. Bayesian learning via stochastic gradient langevin dynamics. In *Proceedings of the 28th international conference on machine learning (ICML-11)*, pp. 681–688, 2011.
- Williams, R. J. Simple statistical gradient-following algorithms for connectionist reinforcement learning. *Machine learning*, 8(3):229–256, 1992.
- Yu, B., Liu, J., and Cui, J. Smart-grpo: Smartly sampling noise for efficient rl of flow-matching models. *arXiv preprint arXiv:2510.02654*, 2025.
- Yuan, H. et al. Reward-directed conditional flow matching. *NeurIPS*, 2024.
- Zhang, F. and Gienger, M. Affordance-based robot manipulation with flow matching. *arXiv preprint arXiv:2409.01083*, 2024.
- Zhang, S., Zhang, W., and Gu, Q. Energy-weighted flow matching for offline reinforcement learning. *arXiv preprint arXiv:2503.04975*, 2025a.
- Zhang, T., Yu, C., Su, S., and Wang, Y. Reinfo: Fine-tuning flow matching policy with online reinforcement learning. *arXiv preprint arXiv:2505.22094*, 2025b.
- Zhong, S., Ding, S., Diao, H., Wang, X., Teh, K. C., and Peng, B. Flowcritic: Bridging value estimation with flow matching in reinforcement learning. *arXiv preprint arXiv:2510.22686*, 2025.

Zhu, X., Cheng, D., Zhang, D., Li, H., Zhang, K., Jiang, C., Sun, Y., Hua, E., Zuo, Y., Lv, X., et al. Flowrl: Matching reward distributions for llm reasoning. *arXiv preprint arXiv:2509.15207*, 2025.

A. Derivation of the Marginal Score for Linear Flow Matching

We derive a closed-form expression for the *marginal* score $\mathbf{s}_t(\mathbf{a}) := \nabla_{\mathbf{a}} \log \rho_t(\mathbf{a})$ along a linear Flow Matching (FM) probability path, conditioned on an observation \mathbf{s} (omitted when clear).

Setup. Let $\mathbf{a}_0 \sim \mathcal{N}(\mathbf{0}, \mathbf{I})$ and $\mathbf{a}_1 \sim p_{\text{data}}(\cdot | \mathbf{s})$. For $t \in [0, 1)$, define the linear interpolation

$$\mathbf{a}_t = (1 - t)\mathbf{a}_0 + t\mathbf{a}_1. \quad (12)$$

Define the per-sample (conditional) target velocity

$$\mathbf{v}^* := \mathbf{a}_1 - \mathbf{a}_0, \quad \text{so that} \quad \mathbf{a}_t = \mathbf{a}_0 + t\mathbf{v}^*. \quad (13)$$

Let $\rho_t(\mathbf{a})$ denote the *marginal* density of \mathbf{a}_t under the joint sampling $\mathbf{a}_0 \sim \mathcal{N}(\mathbf{0}, \mathbf{I})$, $\mathbf{a}_1 \sim p_{\text{data}}(\cdot | \mathbf{s})$.

Step 1: Conditional density and conditional score. Conditioned on \mathbf{a}_1 , (12) becomes an affine transformation of Gaussian noise:

$$\mathbf{a}_t | \mathbf{a}_1 \sim \mathcal{N}(t\mathbf{a}_1, (1 - t)^2\mathbf{I}). \quad (14)$$

Hence the conditional log-density is

$$\log \rho_t(\mathbf{a}_t | \mathbf{a}_1) = -\frac{1}{2(1 - t)^2} \|\mathbf{a}_t - t\mathbf{a}_1\|^2 + C(t), \quad (15)$$

and the conditional score is

$$\nabla_{\mathbf{a}_t} \log \rho_t(\mathbf{a}_t | \mathbf{a}_1) = -\frac{\mathbf{a}_t - t\mathbf{a}_1}{(1 - t)^2}. \quad (16)$$

Step 2: Marginal score as a posterior expectation (no marginal/conditional conflation). The marginal density is $\rho_t(\mathbf{a}_t) = \int \rho_t(\mathbf{a}_t | \mathbf{a}_1) p_{\text{data}}(\mathbf{a}_1 | \mathbf{s}) d\mathbf{a}_1$. Differentiating under the integral sign yields the standard identity:

$$\begin{aligned} \nabla_{\mathbf{a}_t} \log \rho_t(\mathbf{a}_t) &= \frac{1}{\rho_t(\mathbf{a}_t)} \nabla_{\mathbf{a}_t} \int \rho_t(\mathbf{a}_t | \mathbf{a}_1) p_{\text{data}}(\mathbf{a}_1 | \mathbf{s}) d\mathbf{a}_1 \\ &= \int \frac{\rho_t(\mathbf{a}_t | \mathbf{a}_1) p_{\text{data}}(\mathbf{a}_1 | \mathbf{s})}{\rho_t(\mathbf{a}_t)} \nabla_{\mathbf{a}_t} \log \rho_t(\mathbf{a}_t | \mathbf{a}_1) d\mathbf{a}_1 \\ &= \mathbb{E}[\nabla_{\mathbf{a}_t} \log \rho_t(\mathbf{a}_t | \mathbf{a}_1) | \mathbf{a}_t, \mathbf{s}]. \end{aligned} \quad (17)$$

Substituting (16) into (17) gives an exact expression:

$$\mathbf{s}_t(\mathbf{a}_t) = -\frac{\mathbf{a}_t - t \mathbb{E}[\mathbf{a}_1 | \mathbf{a}_t, \mathbf{s}]}{(1 - t)^2}. \quad (18)$$

Step 3: Rewriting in terms of the (marginal) velocity field. Using the path relation $\mathbf{a}_t = (1 - t)\mathbf{a}_0 + t\mathbf{a}_1$, taking conditional expectation given $(\mathbf{a}_t, \mathbf{s})$ yields

$$\mathbb{E}[\mathbf{a}_0 | \mathbf{a}_t, \mathbf{s}] = \frac{\mathbf{a}_t - t \mathbb{E}[\mathbf{a}_1 | \mathbf{a}_t, \mathbf{s}]}{1 - t}. \quad (19)$$

Therefore the posterior mean of the target velocity $\mathbf{v}^* = \mathbf{a}_1 - \mathbf{a}_0$ is

$$\begin{aligned} \mathbb{E}[\mathbf{v}^* | \mathbf{a}_t, \mathbf{s}] &= \mathbb{E}[\mathbf{a}_1 | \mathbf{a}_t, \mathbf{s}] - \mathbb{E}[\mathbf{a}_0 | \mathbf{a}_t, \mathbf{s}] \\ &= \frac{\mathbb{E}[\mathbf{a}_1 | \mathbf{a}_t, \mathbf{s}] - \mathbf{a}_t}{1 - t}. \end{aligned} \quad (20)$$

Plugging (20) into (18) yields an equivalent and often more convenient form:

$$\boxed{\mathbf{s}_t(\mathbf{a}_t) = \frac{t \mathbb{E}[\mathbf{v}^* | \mathbf{a}_t, \mathbf{s}] - \mathbf{a}_t}{1 - t}}. \quad (21)$$

Step 4: Practical estimator via a learned FM velocity field. Flow Matching learns a *marginal* vector field, which (under the standard conditional-to-marginal construction) corresponds to the posterior average of per-sample conditional velocities. Concretely, for the linear path, the optimal marginal velocity satisfies

$$\mathbf{v}_{\text{marg}}(t, \mathbf{a}_t, \mathbf{s}) = \mathbb{E}[\mathbf{v}^* \mid \mathbf{a}_t, \mathbf{s}]. \quad (22)$$

Thus, with a learned FM velocity field $\mathbf{v}_\theta(t, \mathbf{a}_t, \mathbf{s}) \approx \mathbf{v}_{\text{marg}}(t, \mathbf{a}_t, \mathbf{s})$, we obtain the score estimator used in the main text:

$$\boxed{\mathbf{s}_t(\mathbf{a}_t) \approx \frac{t \mathbf{v}_\theta(t, \mathbf{a}_t, \mathbf{s}) - \mathbf{a}_t}{1 - t}}. \quad (23)$$

Asymptotic behavior near $t \rightarrow 1$ and stabilization. The prefactor $(1 - t)^{-1}$ in (23) implies $\|\mathbf{s}_t(\mathbf{a}_t)\| = O((1 - t)^{-1})$ as $t \rightarrow 1$ (for bounded \mathbf{v}_θ). Therefore, the coefficient multiplying the score in the drift should decay as $O(1 - t)$ to keep the score-modulated drift bounded. In ScoRe-Flow, we implement this stabilization by enforcing a hard time-decay in the score scheduler (see Equation (6)), i.e., $\alpha_\psi^{\text{scaled}}(t) \propto (1 - t)$. For score-only baselines where the same schedule also determines the diffusion (Score-SDE), we use linear decay as a canonical instance.

B. Network Architecture Details

Score Scheduler (α_ψ). The score scheduler takes as input only the flow time $t \in [0, 1]$ and outputs a scalar weight $\alpha_\psi(t) > 0$. The architecture consists of a 2-layer MLP and SiLU activations, followed by a Softplus output activation to ensure positivity. A hard time-decay constraint is applied:

$$\alpha_\psi^{\text{scaled}}(t) = (1 - t) \cdot \alpha_\psi(t). \quad (24)$$

This ensures $\alpha_\psi^{\text{scaled}} \rightarrow 0$ as $t \rightarrow 1$, preventing numerical instability from the score function’s $(1 - t)^{-1}$ term

Variance Predictor (σ_ϕ). The variance predictor takes as input the condition embedding $\mathbf{c} \in \mathbb{R}^{d_c}$ from the policy encoder (which encodes observation history). The architecture consists of an MLP with hidden dimensions specified per task (typically [64, 64] for state-based tasks and [256, 256, 256] for vision tasks), using Tanh activations. The output is mapped to a bounded range $[\sigma_{\min}, \sigma_{\max}]$ via:

$$\sigma_\phi = \sigma_{\min} + \frac{\sigma_{\max} - \sigma_{\min}}{2} \cdot (\tanh(\text{MLP}(\mathbf{c})) + 1) \quad (25)$$

Base Velocity Field (\mathbf{v}_θ). We use the same architecture as the pre-trained FM policy, typically a transformer-based architecture for vision tasks or an MLP for state-based tasks. During RL fine-tuning, \mathbf{v}_θ is jointly optimized with $(\alpha_\psi, \sigma_\phi)$.

Initialization. The score scheduler’s final linear layer is initialized with zero weights and bias -2.0 , so that $\text{Softplus}(-2) \approx 0.13$, ensuring small initial α values for training stability.

C. Hyperparameters

In this section, we provide a comprehensive listing of the hyperparameters used for training **ScoRe-Flow** and the **Score-based SDE** baseline. To ensure reproducibility and facilitate a rigorous comparison, we align our base configurations, such as network architectures, optimizer settings, and learning rate schedules, with established baselines (e.g., ReinFlow, DPPO) wherever applicable. The configurations are organized hierarchically: Table 2 outlines the shared parameters common across all tasks, while Table 3, Table 4, and Table 5 detail the specific settings tailored to the unique dynamics of the OpenAI Gym, Franka Kitchen, and Robomimic benchmarks, respectively.

D. Additional Experimental Details

Random Seeds and Variability. We train all RL algorithms using 3 random seeds for all the tasks. The RL fine-tuning curves report the average reward or success rate over these seeds, with shading representing the mean \pm standard deviation to indicate variability between runs.

Table 2. Shared Hyperparameter Configurations for Score-based SDE and ScoRe-Flow.

Parameter	Value (Common to Both)
<i>Optimizer & Learning Rate Settings</i>	
Actor Optimizer	Adam(Kingma, 2014)
Actor LR Weight Decay	0
Actor LR Scheduler	CosineAnnealingWarmupRestart(Loshchilov & Hutter, 2016)
Actor LR Cycle Steps	100*
Critic Optimizer	Adam
Critic LR Scheduler	CosineAnnealingWarmupRestart
Critic Scheduler Warmup	10
Critic LR Cycle Steps	100†
<i>Network Architecture & Training</i>	
Policy Network Architecture	512 × 3 MLP
Critic Network Architecture	256 × 3 MLP
Critic Loss Coef.	0.50
Reward Scale	1.0
Reward Normalization	True

*Set to 150 for the Franka Kitchen-Partial task.

†Set to 50 for the Franka Kitchen-Partial task.

Rendering Backend. To accelerate GPU-based computation during training and wall-time testing, we set the MuJoCo graphics rendering backend (MUJOCO.GL) to the Embedded System Graphics Library (EGL). We note that users relying on software rendering (e.g., `osmesa`) or running multiple threads on shared CPU/GPU kernels may experience longer compute times than those reported in our benchmarks.

Wall-clock Time Analysis. For fair comparison, wall-clock time is measured sequentially on a single NVIDIA RTX 3090 GPU with EGL rendering for all tasks, with the exception of Robomimic Transport where two A100 GPUs are employed. We calculate the total wall-clock time by multiplying the average iteration time by the total number of iterations.

Quantitative results highlight the efficiency of our method: ScoRe-Flow reaches 90% of final performance in only **0.16 hours on average** for D4RL tasks. This represents a **22× speedup** compared to DPPO (3.48 hours), which typically requires 50 to 100 denoising steps. This efficiency stems from our use of fewer denoising steps ($K = 4$) and the effective guidance of score-based mean control.

While FQL shows shorter per-iteration times, it is not necessarily more efficient overall: its batch size is considerably smaller than PPO-based methods, and it requires significantly more total training iterations to converge. Furthermore, FQL lacks the parallel computing design inherent to DPPO and ReinFlow.

Performance Metrics. We employ tailored metrics to rigorously evaluate performance across different domains:

- (i) **Episode Reward (D4RL Locomotion):** This metric represents the unnormalized cumulative return accumulated over an episode, serving as a direct proxy for the agent’s gait quality, stability, and energy efficiency in continuous control tasks. Higher rewards indicate more proficient locomotion. On this benchmark, ScoRe-Flow demonstrates superior asymptotic performance, particularly in high-dimensional state spaces. Notably, on the challenging `Humanoid-v3` task, our method achieves a state-of-the-art reward of **5100±47**, significantly surpassing strong baselines such as ReinFlow-R (5041) and DPPO (5001), highlighting its capability to master complex dynamics.
- (ii) **Success Rate (Robomimic):** Defined as the percentage of evaluation rollouts that satisfy the goal condition by the final timestep, this metric quantifies the reliability and precision of the policy in visual manipulation settings. ScoRe-Flow consistently dominates this metric, exhibiting exceptional robustness in mapping high-dimensional pixel inputs to precise actions. Specifically, it achieves a remarkable **98.3%** success rate on the `PickPlaceCan` task and maintains the highest average success rate (**92.5%**) across the suite, outperforming the best baseline by a margin of 5.4%.
- (iii) **Completed Subtasks (Franka Kitchen):** For this multi-stage manipulation benchmark, we report the average number of successfully completed subtasks out of a maximum of 4 per episode. This metric reflects the policy’s capacity

Table 3. Detailed Hyperparameter Settings for OpenAI Gym Locomotion Tasks.

(a) Shared and Algorithm-Specific Base Hyperparameters

Parameter	Score-based SDE	ScoRe-Flow
<i>PPO Optimization Configurations</i>		
PPO Clip Ratio (ϵ_{clip})		0.01
Target KL Divergence		1.0
Entropy Coef. (α)		0.03
Num. Parallel Envs		40
Batch Size		50,000
Update Epochs		5
Discount Factor (γ)		0.99
GAE Lambda(Schulman et al., 2015) (λ)		0.95
Action Chunking Size(Lai et al., 2022)		4
Condition Stacking		1
Denoising Steps (K)		4
BC Loss Coef (β)		0.01
Clip Interm. Actions		True
Max Ep. Steps / Rollout Steps		1000 / 500
<i>Exploration Mechanism</i>		
Exploration Noise Type	ϵ -SDE Stochastic	Learnable Noise Scheduler
Exploration ϵ_t Schedule	Linear Decay	N/A
Noise Hold Ratio	N/A	35% of total iteration
Noise Decay Target	N/A	$0.3\sigma_{\min} + 0.7\sigma_{\max}$
<i>Score Parameters</i>		
Learnable Score Scheduler	N/A	MLP
Score Scheduler Hidden Dim	N/A	16

(b) Task-Specific Hyperparameters: ScoRe-Flow

Parameter	Hopper-v2	Walker2d-v2	Ant-v0	Humanoid-v3
Min / Max Noise Std (σ)	0.10 / 0.24	0.10 / 0.24	0.08 / 0.16	0.08 / 0.16
Critic Warmup Iters	0	5	0	0
Actor LR (Cosine)	$\cos(4.5e-5, 2e-5)$	$\cos(4e-4, 4e-4)$	$\cos(4.5e-5, 2e-5)$	$\cos(4.5e-5, 2e-5)$
Critic LR (Cosine)	$\cos(6.5e-4, 3e-4)$	$\cos(4e-3, 4e-3)$	$\cos(6.5e-4, 3e-4)$	$\cos(6.5e-4, 3e-4)$
Total Training Iters	1001	1001	1001	201

(c) Task-Specific Hyperparameters: Score-based SDE

Parameter	Hopper-v2	Walker2d-v2	Ant-v0	Humanoid-v3
Base Exploration Coef. (ϵ_0)	0.1	0.1	0.01	0.01
Critic Warmup Iters	0	3 to 5	3 to 5	3 to 5
Actor LR (Cosine)	$\cos(4.5e-5, 2e-5)$	$\cos(4e-4, 4e-4)$	$\cos(4e-4, 2e-4)$	$\cos(4.5e-5, 2e-5)$
Critic LR (Cosine)	$\cos(6.5e-4, 3e-4)$	$\cos(4e-3, 4e-3)$	$\cos(4e-3, 2e-3)$	$\cos(6.5e-4, 3e-4)$
Total Training Iters	1001	1001	1001	201

for long-horizon sequential reasoning and its ability to overcome sparse reward signals. ScoRe-Flow excels in this setting, achieving the highest average completion rate of **3.60**. Notably, it attains a perfect score of 4.0 on the hardest Kitchen-Complete task and demonstrates substantial improvements on the Partial dataset by surpassing ReinFlow with a score of 3.8 against 3.4, proving its effectiveness in chaining complex behaviors.

Ablation Studies. We analyze the impact of denoising steps (K) and the decoupled variance prediction mechanism.

- (i) *Denoising Steps:* Performance varies across different K settings. Through this ablation, we determine the **optimal** K configuration that balances accuracy and efficiency. Specifically, we identify the minimal steps required to maintain peak performance, ensuring that the system operates at maximum speed without compromising precision.
- (ii) *Variance Prediction (Score-SDE):* To isolate the contribution of decoupled variance prediction, we compare ScoRe-Flow

Table 4. Hyperparameter Configurations for Franka Kitchen Tasks.

(a) Shared and Algorithm-Specific Base Hyperparameters

Parameter	Score-based SDE	ScoRe-Flow
<i>PPO Optimization Configurations</i>		
PPO Clip Ratio (ϵ_{clip})		0.01
Target KL Divergence		1.0
Update Epochs		10
Discount Factor (γ)		0.99
GAE Lambda (λ)		0.95
Num. Parallel Envs		40
Batch Size		5600
Total Training Iters		301
Action Chunking Size		4
Condition Stacking		1
Denoising Steps (K)		4
Clip Intern. Actions		True
Random / Denoised Clip Value		3.0 / 1.0
BC Loss Coef (β)		0.00
Critic Weight Decay		1×10^{-5}
Critic Warmup Iters		0
<i>Exploration Mechanism</i>		
Exploration Noise Type	ϵ -SDE Stochastic	Learnable Noise Scheduler
Exploration ϵ_t Schedule	Linear Decay	N/A
Noise Hold Ratio	N/A	100% of total iteration
Noise Decay Target	N/A	σ_{max}
<i>Score Parameters</i>		
Learnable Score Scheduler	N/A	MLP
Score Scheduler Hidden Dim	N/A	16

(b) Task-Specific Hyperparameters: ScoRe-Flow

Parameter	Complete	Mixed	Partial
Finetuning Denoising Steps	4	4	8
Min / Max Noise Std (σ)	0.05 / 0.12	0.05 / 0.12	0.05 / 0.35
Entropy Coef (α)	0.00	0.00	0.01
Actor LR (Cosine)	$\cos(4.5e-5, 2e-5)$	$\cos(4.5e-5, 2e-5)$	$\cos(4.5e-5, 2e-5)$
Critic LR (Cosine)	$\cos(6.5e-4, 3e-4)$	$\cos(6.5e-4, 3e-4)$	$\cos(6.5e-4, 3e-4)$

(c) Task-Specific Hyperparameters: Score-based SDE

Parameter	Complete	Mixed	Partial
Base Exploration Coef. (ϵ_0)	0.01 to 0.1	0.01	0.05
Entropy Coef (α)	0.00	0.00	0.00
Actor LR (Cosine)	$\cos(4.5e-5, 2e-5)$	$\cos(4.5e-5, 2e-5)$	$\cos(4.5e-5, 2e-5)$
Critic LR (Cosine)	$\cos(6.5e-4, 3e-4)$	$\cos(6.5e-4, 3e-4)$	$\cos(2e-4, 5e-5)$

against **Score-SDE** (as formulated in Eq. 11). In this ablation, the diffusion coefficient is strictly coupled to the drift without learned variance. We employ the linear decay schedule for the weighting term $\lambda(t)$, where its value decreases linearly from λ_{max} to 0 on the trajectory. This imposes a rigid noise annealing profile: strong exploration at the beginning ($t = 0$) and deterministic execution at the end ($t = 1$). While this fixed schedule enables faster initial convergence in some tasks due to immediate guidance, it lacks the adaptability of ScoRe-Flow’s learned variance, consistently yielding lower asymptotic performance. This trade-off is empirically evident in the learning curves in Section 5.3 (see Figures 2, 3 and 4), where Score-SDE typically rises rapidly in the early stages, but plateaus at a lower performance level compared to ScoRe-Flow.

Table 7 outlines the specific flow matching architectures employed across our benchmarks. Adhering to the experimental

Table 5. Hyperparameter Configurations for Robomimic Image-input Manipulation Tasks.

(a) Shared and Algorithm-Specific Base Hyperparameters

Parameter	Score-based SDE	ScoRe-Flow
<i>PPO Optimization Configurations</i>		
PPO Clip Ratio (ϵ_{clip})		0.01
Target KL Divergence		0.01
Update Epochs		10
Discount Factor (γ)		0.999
GAE Lambda (λ)		0.95
Num. Parallel Envs		50
Batch Size		500
Condition Stacking		1
Clip Intern. Actions		True
Random / Denoised Clip Value		3.0 / 1.0
BC Loss Coef (β)		0.00
Max Grad Norm		25.0
<i>Exploration Mechanism</i>		
Exploration Noise Type	ϵ -SDE Stochastic	Learnable Noise Scheduler
Exploration ϵ_t Schedule	Linear Decay	N/A
Noise Scheduler Type	N/A	Learnable Decay
Noise Hold Ratio	N/A	100% of total iteration
Noise Decay Target	N/A	σ_{max}
<i>Score Parameters</i>		
Learnable Score Scheduler	N/A	MLP
Score Scheduler Hidden Dim	N/A	16

(b) Task-Specific Hyperparameters: ScoRe-Flow

Parameter	Can	Square	Transport
Total Training Iters	151	301	201
Action Chunking Size	4	4	8
Denoising Steps (K)	1	4	4
Min / Max Noise Std (σ)	0.08 / 0.14	0.08 / 0.14	0.05 / 0.10
Entropy Coef (α)	0.01	0.01	0.01
Critic Warmup Iters	5	5	5
Actor LR (Cosine)	cos(2e-5, 1e-5)	cos(3.5e-6, 3.5e-6)	cos(3.5e-6, 3.5e-6)
Critic LR (Cosine)	cos(6.5e-4, 3e-4)	cos(4.5e-4, 3e-4)	cos(3.2e-4, 3e-4)
Critic Weight Decay	0	0	1e-5

(c) Task-Specific Hyperparameters: Score-based SDE

Parameter	Can	Square	Transport
Total Training Iters	151	301	201
Action Chunking Size	4	4	8
Denoising Steps (K)	1	2	4
Max Episode Steps	300	400	800
Num. Rollout Steps	300	400	400
Base Exploration Coef. (ϵ_0)	0.01	0.01	0.01
Entropy Coef (α)	0	0	0
Critic Warmup Iters	2	2	5
Actor LR (Cosine)	cos(2e-5, 1e-5)	cos(3.5e-6, 3.5e-6)	cos(3.5e-6, 3.5e-6)
Critic LR (Cosine)	cos(6.5e-4, 3e-4)	cos(4.5e-4, 3e-4)	cos(3.2e-4, 3e-4)
Critic Weight Decay	0	0	1e-5

protocols established by ReinFlow (Zhang et al., 2025b), we perform a task-adaptive architectural selection for each domain, choosing the optimal variant (either Rectified Flow or the Shortcut Model) as detailed in the table. This approach ensures that the flow matching formulation is tailored to the intrinsic dynamics of each environment. By aligning the model backbone with the specific complexities of the tasks, which range from standard locomotion to high-dimensional manipulation, we

Table 6. Per Iteration Wall-clock Time Analysis on D4RL OpenAI Gym Locomotion Tasks (Seconds). Comparison of single training iteration time across three random seeds. ScoRe-Flow maintains competitive computational efficiency compared to flow-based baselines, with only negligible overhead introduced by the variance prediction mechanism.

Task	Method	Single Iteration (s)			Mean \pm Std
		S1	S2	S3	
Hopper-v2	ReinFlow-R	11.598	11.704	11.843	11.715 \pm 0.123
	ReinFlow-S	12.051	12.127	12.372	12.290 \pm 0.141
	DPPO	99.502	99.616	98.021	99.046 \pm 0.890
	FQL	4.373	4.366	4.515	4.418 \pm 0.084
	Score-SDE	11.652	11.715	11.793	11.720 \pm 0.071
	ScoRe-Flow	11.821	11.904	11.885	11.870 \pm 0.043
Walker2d-v2	ReinFlow-R	11.861	11.446	11.382	11.563 \pm 0.260
	ReinFlow-S	12.393	12.690	13.975	13.019 \pm 0.841
	DPPO	101.15	106.12	98.470	101.91 \pm 3.884
	FQL	5.248	4.597	5.207	5.017 \pm 0.365
	Score-SDE	11.605	11.524	11.588	11.572 \pm 0.043
	ScoRe-Flow	11.782	11.845	11.751	11.793 \pm 0.048
Ant-v0	ReinFlow-R	17.210	17.685	17.524	17.473 \pm 0.242
	ReinFlow-S	17.291	17.821	18.090	17.734 \pm 0.407
	DPPO	102.36	104.63	99.042	102.01 \pm 2.811
	FQL	5.242	4.950	5.309	5.167 \pm 0.191
	Score-SDE	17.355	17.422	17.501	17.426 \pm 0.073
	ScoRe-Flow	17.653	17.712	17.805	17.723 \pm 0.077
Humanoid-v3	ReinFlow-R	31.437	30.223	31.088	30.916 \pm 0.625
	ReinFlow-S	30.499	30.058	31.029	30.529 \pm 0.486
	DPPO	109.88	105.45	113.35	109.56 \pm 3.961
	FQL	5.245	4.981	5.522	5.249 \pm 0.271
	Score-SDE	30.852	30.924	31.055	30.944 \pm 0.103
	ScoRe-Flow	31.251	31.185	31.320	31.252 \pm 0.068

establish a rigorous and fair baseline for comparison.

Table 7. Flow Matching Model Variants Configuration. We select the specific model architecture (Rectified Flow vs. Shortcut Model) for each task to achieve optimal performance, aligning with the baseline configurations reported in ReinFlow for a fair comparison.

Domain	Task / Dataset	Model Framework	Rationale
Locomotion	OpenAI Gym (All Tasks)	Rectified Flow	Performance
	Franka Kitchen (All Tasks)	Shortcut Model	Performance
Manipulation	Robomimic Can	Rectified Flow	Performance
	Robomimic Square	Rectified Flow	Performance
	Robomimic Transport	Shortcut Model	Efficiency & Performance

E. Extended Results with 5-Seed Significance Tests

We expand all experiments to 5 random seeds and report statistical significance via Welch’s t-test (Welch, 1947). Table 8 and Table 9 show the updated results. Across 45 pairwise comparisons, ScoRe-Flow achieves 18 statistically significant wins ($p < 0.05$) and **zero significant losses**. Results are highly consistent with the original 3-seed report: means shift by at most 1–2%, and all rankings are preserved.

F. Ablation Studies: Score Term, Schedule, and Coupling

We perform three ablation experiments to isolate the contribution of each component. All ablations use the same backbone, PPO hyperparameters, and variance network as ScoRe-Flow; only the specified component is modified.

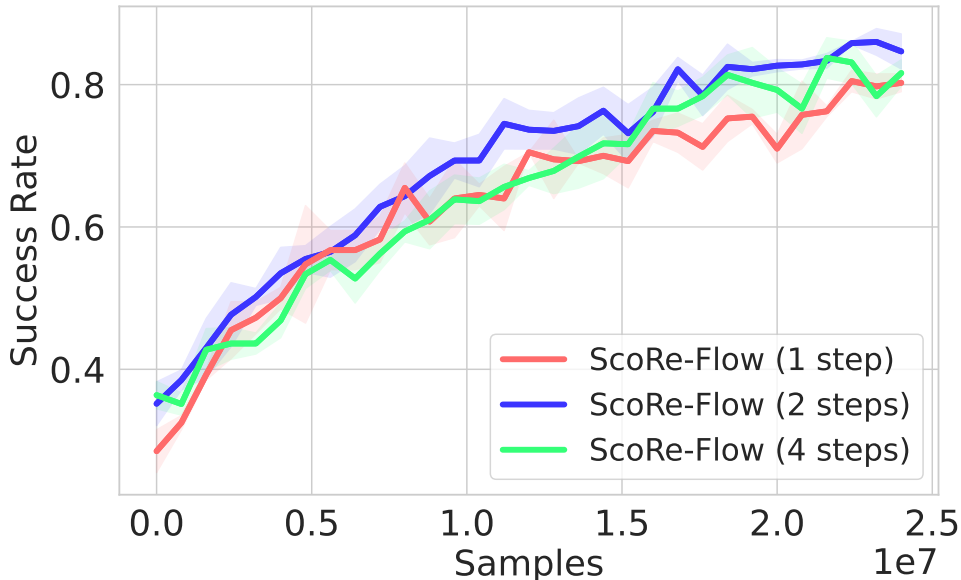


Figure 8. **Ablation study on denoising steps (K).** We evaluate the success rate on the Robomimic Square task across varying inference steps ($K \in \{1, 2, 4\}$). The results demonstrate that the success rate reaches its maximum at $K = 2$, outperforming both the 4-step and 1-step settings, thus identifying $K = 2$ as the optimal inference configuration.

Table 8. 5-seed D4RL results (mean \pm std). \dagger : $p < 0.05$ vs ScoRe-Flow (Welch’s t-test).

Method	Hopper	Walker2d	Ant	Humanoid
DPPO	3275 \pm 24	3897 \pm 76 \dagger	3951 \pm 30 \dagger	4873 \pm 0
FQL	3032 \pm 65 \dagger	3709 \pm 14 \dagger	620 \pm 3 \dagger	2334 \pm 61 \dagger
ReinFlow-R	3204 \pm 44	4092 \pm 14	4021 \pm 31	4976 \pm 26 \dagger
ReinFlow-S	3253 \pm 29	4202 \pm 32	4119 \pm 53	4956 \pm 110
Score-SDE	3155 \pm 91	3922 \pm 78 \dagger	3975 \pm 51 \dagger	4928 \pm 113 \dagger
ScoRe-Flow	3235\pm34	4189\pm145	4096\pm87	5125\pm47

$\alpha = 0$ (**No score correction**). Removing the score term ($\alpha_\psi = 0$) while retaining \mathbf{v}_θ finetuning and learned variance yields performance comparable to ReinFlow under matched settings. On Kitchen-Complete, $\alpha = 0$ reaches 0.98 with slower early convergence (vs ScoRe-Flow 0.99). On Humanoid, $\alpha = 0$ converges noticeably slower (5000 vs 5125). This confirms the score provides independent benefit beyond \mathbf{v}_θ finetuning.

$\alpha = 1$ (**Fixed full-strength score**). Setting $\alpha_\psi = 1$ (bypassing the learned scheduler) severely degrades performance: Kitchen-Complete drops to 0.50, and Humanoid convergence slows approximately $3\times$ with high variance. The score magnitude diverges as $O((1-t)^{-1})$ near $t = 1$; without learned attenuation, it overwhelms the PPO optimization signal. The learned α_ψ is necessary.

$\Lambda = \text{MLP}$ (**Coupled learned Score-SDE**). Replacing the decoupled architecture with a coupled-but-learned variant (a single MLP predicting tied drift-variance) produces results *worse than even fixed- σ Score-SDE*: Kitchen-Complete degrades to 0.93 (vs 0.97 for fixed Score-SDE, 0.99 for ScoRe-Flow), and Transport drops to 0.50 (vs 0.94 for ScoRe-Flow). This confirms that decoupled control over drift and variance is essential.

G. Score Scheduler Analysis

Figure 9 shows the learned $\alpha_\psi(t)$ behavior across training. The scheduler converges systematically: it applies stronger score correction at early denoising steps (small t) where \mathbf{v}_θ predictions are less reliable, and reduces toward zero near $t = 1$, consistent with the $(1-t)$ boundary decay. Over the course of training, the overall magnitude of α_ψ decreases as \mathbf{v}_θ improves through RL finetuning, confirming that the score’s corrective role diminishes as the policy becomes well-calibrated.

Table 9. 5-seed Robomimic (success rate) and Kitchen (tasks completed) results. †: $p < 0.05$.

Method	Can	Square	Transport	K-Complete	K-Mixed	K-Partial
DPPO	.993±.006	.771±.033	.528±.459	3.78±.17	3.40±.54	3.48±.47
ReinFlow-S	.978±.003	.744±.047	.888±.030	3.92±.03	2.99±.01	3.39±.54
Score-SDE	.957±.019	.778±.024†	.896±.060	3.97±.01	2.99±.01	3.18±.45†
ScoRe-Flow	.979±.020	.835±.032	.940±.022	3.96±.02	3.00±.01	3.98±.02

The α_ψ scheduler adds only 800 parameters (0.02% of the 4.74M total), introducing negligible computational overhead.

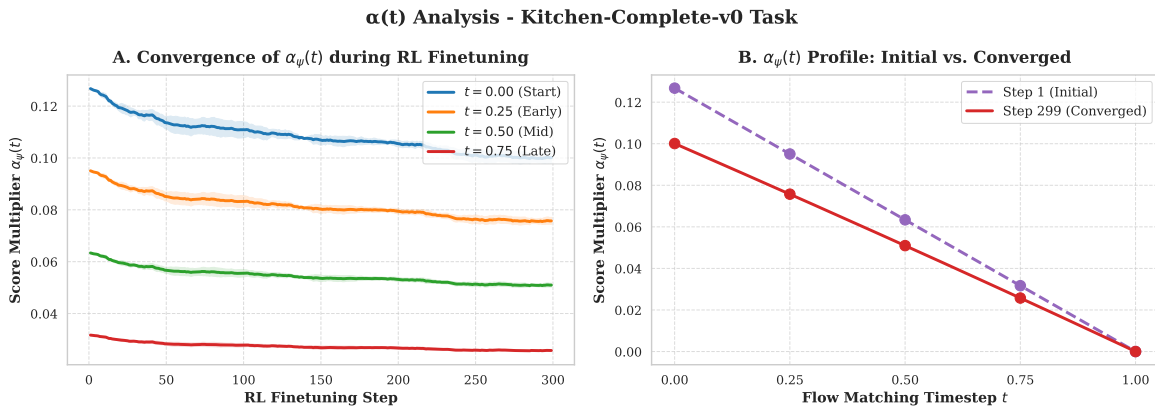


Figure 9. Learned $\alpha_\psi(t)$ scheduler behavior. **Left:** α_ψ as a function of denoising time t at different training stages. The scheduler applies stronger correction early in denoising and reduces near $t = 1$. **Right:** Overall α_ψ magnitude decreases over training as v_θ improves.